Correlation of structure and magnetism of ultrathin Co films on Pd(001) prepared by thermal and pulsed laser deposition

H. L. Meyerheim,* M. Przybylski, A. Ernst, Y. Shi, J. Henk, E. Soyka, and J. Kirschner
Max-Planck-Institut für Mikrostrukturphysik, Weinberg 2, D-06120 Halle, Germany
(Received 2 January 2007; revised manuscript received 23 March 2007; published 20 July 2007)

We present a combined experimental and theoretical analysis of the atomic structure and the magnetic properties of 1- and 2-monolayer (ML)-thick Co films on Pd(001) grown by thermal deposition (TD) and pulsed laser deposition (PLD). While surface x-ray diffraction measurements show that the geometric structures of the as-deposited samples differ depending on the deposition method (alloy formation for PLD versus epitaxial growth for TD), magneto-optic Kerr-effect loops indicate an in-plane easy magnetization axis independent of the preparation method. Annealing at 600 K induces a reorientation of the easy magnetization axis from in-plane to out of plane. This goes in parallel with substantial structural reorganization, leading to a Co/Pd multilayer structure with a top Pd layer. In agreement with experiments, fully relativistic Kohn-Korringa-Rostoker calculations including experimentally derived structural relaxations and disorder predict in-plane magnetization for the as-grown samples and out-of-plane magnetization for the annealed 2 ML sample characterized by an (incomplete) Pd/Co/Pd/Co/Pd(001) layer sequence. However, in-plane magnetization for the 1 ML Pd/Co/Pd(001) sandwich is theoretically predicted. Our study emphasizes the decisive importance of structural order, relaxation, and interface contribution to the magnetic anisotropy energy.

DOI: 10.1103/PhysRevB.76.035425 PACS number(s): 68.35.Ct, 61.10.−i, 75.70.Ak

I. INTRODUCTION

Ordered CoPd and CoPt alloys are intensely investigated due to their potential applications in high-density magnetic storage devices.[1,2] In this context, perpendicular magnetic anisotropy (PMA) is of particular interest and was reported in both thick films[3–5] and multilayers.[6–8]

While PMA is, in general, attributed to the surface and interface contributions to the total magnetocrystalline anisotropy energy (MAE), in these alloys it is an intrinsic bulk property. For comparison, bulk MAE's equal to several μeV/atom, but those of ordered CoPt alloys ($L1_0$-type structure) were calculated to be larger by 2 orders of magnitude,[9] in good agreement with experimentally derived values [e.g., 58 versus 130 μeV/atom (Ref. 10)].

Despite an abundance of studies, a clear picture relating PMA to the atomic alloy and/or multilayer structure has not yet evolved. For instance, in the experimental study of Engel *et al.*[6] a crossover from out-of-plane to in-plane magnetization in Co/Pd(001) superlattices between one and two atomic layers of Co was determined, but calculations using the fully relativistic spin-polarized screened Kohn-Korringa-Rostoker (KKR) method predict PMA only for superlattices on Pd(111) but not on Pd(001).[11] These theoretical results are at variance with those of Wang *et al.*, proposing PMA for the Pd/Co/Pd(001) sandwich.[12,13]

The calculations of Pustogowa *et al.*[11] as well as of Wang *et al.*[12,13] are based on "unrelaxed" and nonalloyed interface structures. The Co atoms are placed on the fcc-Pd(001) substrate and adopt the Pd interlayer spacing (1.945 Å), an assumption which is hardly fulfilled considering the almost 10% lattice mismatch between Pd (2.75 Å) and fcc-Co (2.50 Å).[14] In this context, an inward relaxation of the Co atoms leading to a reduced Co-Pd bonding length was predicted to enhance the PMA due to the increased Co-Pd hybridization.[12,13] On the other hand, any intermixing and the presence of structural defects were reported to reduce the PMA.[15,16]

From these examples, it is evident that the precise knowledge of the geometric alloy and interface structure is decisive for understanding the physical origin of the PMA in Co/Pd superlattices and alloys. By contrast, only a few quantitative studies were carried out thus far. Examples are polarized Co *K*-edge extended x-ray absorption fine structure studies on (111)-oriented Co/Pd superlattices.[17–19]

Similarly, for (001)-oriented Pd, no systematic analysis of the magnetic properties and their relation with the Co/Pd interface structure exists. Only several experiments were carried out to study the growth and interface formation of room-temperature (RT) deposited and annealed Co/Pd(001).[20–22]

In contrast to the (111)-oriented surfaces, where a tendency to spontaneously alloy at RT was determined[18,19,23] and theoretically predicted for both orientations [(001) and (111)],[24] x-ray photoelectron diffraction, low-energy ion scattering,[20,21] and quite recent surface x-ray diffraction (SXRD) experiments combined with atomic-scale simulations[22] did not find evidence of interface mixing for thermally deposited Co/Pd(001) at RT. The calculations in Ref. 22 indicated that—although alloy formation is thermodynamically favored—the activation barrier for site exchange is equal to 0.4 eV, preventing alloy formation for Co films prepared by thermal deposition (TD). By contrast, for Co atoms deposited by pulsed laser deposition (PLD),[25,26] substantial alloying was observed. This is attributed to the higher kinetic energy (up to several eV) of the deposited atoms.

In summary, these studies indicated substantial differences of the evolving interface structure depending on the preparation method (TD versus PLD), though their impact on the magnetic properties is unknown. In addition, since the as-deposited samples correspond to phases far from equilibrium, the impact of annealing on both structure and magne-

tism is a key to understanding their relation, especially in the context of possible technological applications.

To this end, we have carried out a combined experimental and theoretical study on 1- and 2-monolayer (ML)-thick Co films on Pd(001) prepared by TD and PLD before and after annealing. Magneto-optical Kerr-effect (MOKE) measurements indicate that, while for the as-deposited samples in-plane magnetization is found in any case, annealing up to 600 K induces a spin-reorientation transition from in plane to out of plane. This goes in parallel with the formation of an ordered Pd/Co sandwich structure with a Pd top layer. In agreement with the experiments, *ab initio* numerical simulations within the density-functional theory (DFT) predict an in-plane easy axis for *all* as-deposited samples and PMA for the (not completely ordered) double sandwich structure Pd/Co/Pd/Co/Pd(001) formed by annealing 2 ML Co/Pd(001). Some discrepancy exists in the case of 1 ML samples, where calculations predict in-plane magnetization.

II. EXPERIMENTS

Scanning tunneling microscopy (STM) and MOKE experiments were carried out in a multichamber ultrahigh vacuum (UHV) system (base pressure of 5×10^{-11} mbar). Prior to Co deposition, the Pd(001) single-crystal surface was cleaned by repeated cycles of Ar^+-ion sputtering (2 keV) followed by annealing at 950 K until no traces of contaminants could be detected by Auger electron spectroscopy (AES). Simultaneously, low-energy electron diffraction (LEED) showed sharp and well-contrasted spots, while atomically flat terraces several 100 nm wide were observed in the STM images.

Co was deposited by TD using a Co rod heated by electron bombardment. For PLD, a KrF excimer laser (248 nm wavelength, 34 ns pulse length, repetition rate 10 Hz, and pulse energy $\approx$325 mJ) was focused on a Co target about 120 mm away from the sample surface. An average deposition rate between 0.1 and 0.3 ML/min is achieved, comparable to the deposition rate for TD. We refer to 1 ML as one adatom per substrate atom, i.e., 1.32×10^{15} atoms/cm^2. In all cases, the substrate crystal was kept at room temperature during deposition.

STM images were recorded in the constant current mode at 0.2–0.5 V tip bias voltage and 0.1–0.5 nA tunneling current. Longitudinal and polar MOKE experiments were carried out by using a *p*-polarized laser beam ($\lambda=675$ nm) incident on the sample at an angle of 67° and 5°, respectively. By using the modulation technique as outlined in Ref. 27, and collecting the 2*f* frequency, a signal is recorded proportional to the Kerr rotation.

A separate UHV chamber was used for collecting the SXRD reflection intensities, also allowing *in situ* sample preparation by TD and PLD as well as characterization by LEED and AES. Before and after the SXRD experiments, AES spectra were collected to control sample cleanliness and to cross-check the Co-film thickness with the SXRD-derived total amount of Co. Within an error of about 0.15 ML, SXRD and AES correlate. The detailed setup for the SXRD measurement is described elsewhere.[28,29]

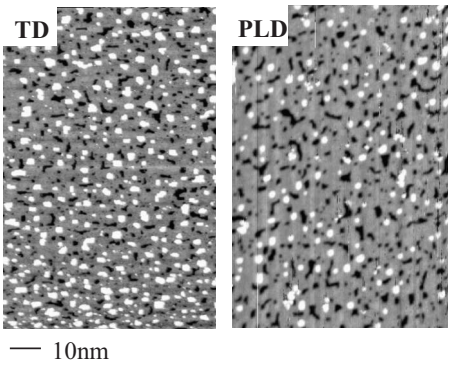

FIG. 1. STM images for 1.1 ML Co deposited by TD (left) and 1.0 ML Co deposited by PLD (right). The length scale is shown at the lower left.

X rays were generated by a rotating anode system and monochromatized (Cu $K\alpha$ radiation) by using a focusing multilayer monochromator yielding a peak count rate of 430 counts/s at the (1 0 0.05) reflection. This position is close to the (100) antiphase condition along the (10ℓ) crystal truncation rod (CTR).[14,30,31] The CTR's arise from the truncation of the crystal; therefore, the coordinate ℓ of the normal momentum transfer $q_z=\ell\times c^\star$ becomes a continuous parameter [$c^\star=1.59$ Å^{-1} is the reciprocal lattice unit (rlu) of Pd along q_z].[32] The detailed calculation shows that at the (100) position the scattered intensity of the whole (semi-infinite) crystal is proportional to a quarter of a Pd monolayer, i.e., $I(100)\propto(f_{\mathrm{Pd}})^2/4$, where f_{Pd} is the atomic scattering factor of Pd.

Integrated x-ray reflection intensities were collected under total reflection conditions of the incoming beam (incidence angle $\alpha_i\approx0.32°$) by rotating the sample about its surface normal.[30,31]

III. ANALYSIS OF THE INTERFACE STRUCTURE

A. Scanning tunneling microscopy

At first we discuss the growth of Co on Pd(001) on the basis of STM. The left and right panels in Fig. 1 show STM images obtained after Co deposition by TD and PLD, respectively. The coverage for the sample prepared by TD is slightly higher (1.1 ML) than for the PLD sample (1.0 ML), but the gross features of the images are identical. Both films exhibit a three-layer structure. Dark, gray, and white areas correspond to the Pd substrate and to the first and second Co layers, respectively. Layer-by-layer growth is not perfect; there is a 10%–20% second-layer occupancy, while the substrate is covered only 80%–90% of first-layer atoms. The island size within the topmost layer is in the 3–5 nm range. In summary, the STM images do not indicate pronounced differences between the TD and PLD prepared samples.

B. Surface x-ray diffraction

Despite the similarity of the STM images of the as-deposited samples, the SXRD measurements provide direct evidence for substantial dependence of the interface structure

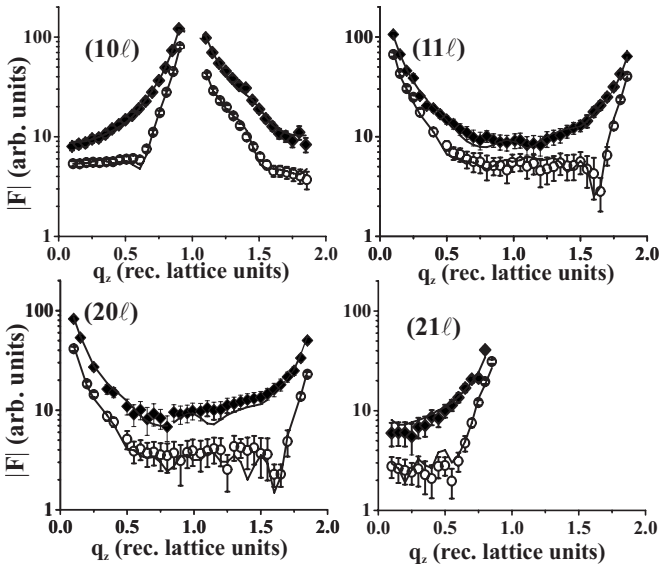

FIG. 2. Measured (symbols) and calculated (lines) structure factor amplitudes along the (10ℓ), (11ℓ), (20ℓ), and (21ℓ) CTR's for 1 ML Co deposited on Pd(001) by TD (filled diamonds) and PLD (open circles). Curves are shifted for clarity.

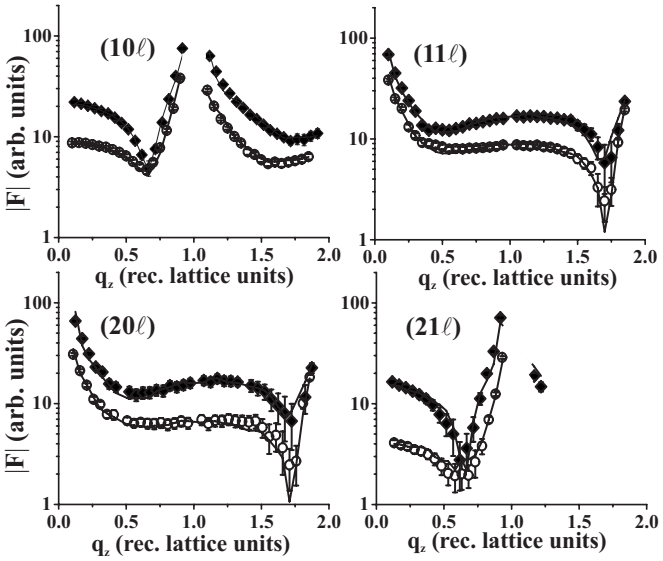

FIG. 3. Measured (symbols) and calculated (lines) structure factor amplitudes for 1 ML Co deposited on Pd(001) by TD (filled diamonds) and PLD (open circles) after annealing at 600 K for 15 min. Curves are shifted for clarity.

on the preparation method as discussed in the following.

The structure factor amplitudes were derived from the integrated intensities after correcting for geometric factors.[33] Standard deviations (σ) of the $|F|$'s were derived from the counting statistics and the reproducibility of symmetry equivalent reflections.[30,31] They are represented by the error bars.

Figure 2 shows on a logarithmic scale the structure factor amplitudes, $|F|$, along the (10ℓ), (11ℓ), (20ℓ), and (21ℓ) CTR (Ref. 14) for the as-deposited samples with a Co coverage of 1.00 ± 0.15 ML. Filled diamonds and open circles represent CTR's collected for samples prepared by TD and PLD, respectively.

While for the as-deposited samples even direct inspection reveals significant differences between the CTR's depending on the preparation method, after 15 min annealing at 600 K the CTR's are very similar, indicating a close correspondence between the structures. The CTR's of the annealed samples are shown in Fig. 3, where filled diamonds and open circles represent the measured $|F|$ for the TD and PLD samples.

Each data set consists of about 120 symmetry-independent reflections. The CTR's were measured up to the normal momentum transfer $q_z=1.85$ rlu. Bulk Bragg reflections correspond to the condition: $h+k+\ell=2n$ (n=integer); i.e., they are located at $\ell=1$ along the (10ℓ) and (21ℓ) rods, and at $\ell=0$ and $\ell=2$ along the (11ℓ) and (20ℓ) rods.

Direct inspection of the intensity distribution along the rods allows several qualitative conclusions. First, within each data set, the (10ℓ) and (21ℓ) rods as well as the (11ℓ) and (20ℓ) rods exhibit the same overall shape along q_z, although they differ on an absolute intensity scale. This indicates that the adatoms occupy high-symmetry sites only. Pd and Co atoms are located either at $(x,y)=(0,0)$ or at $(1/2,1/2)$, alternating layer by layer leading to the same in-plane phase factor, $\exp[i2\pi(hx+ky)]$, for the corresponding rods of each pair.

The quantitative analysis was carried out by least-squares refinement of the calculated $|F|$'s to the experimental ones. Since there is only one independent atomic position within the two-dimensional unit cell, only one z parameter and one Debye parameter (B) representing disorder (static and dynamic) need to be refined for each layer. Different alloy compositions are simulated by varying the site occupancy of Co (Θ_{Co}) and Pd (Θ_{Pd}), with the boundary condition $\Theta_{\mathrm{Co}}+\Theta_{\mathrm{Pd}}=1$ in the case of complete layers. Since a maximum of six layers is sufficient to achieve fit convergence, at most 10–15 parameters are required to model the interface structure. In comparison with the number of data points ($\approx$120), this is a number low enough to ensure a sufficient overdetermination of the refinement problem.

In the least-squares refinement, the correlation (C) between the parameters is also decisive. A large number of high correlations (e.g., $|C|>0.8$) between parameters can severely affect the fit convergence, its quality, and the standard deviations of the parameters derived from the variance-covariance matrix.[34] In this study as well as in a number of other ones concerned with interface structures on similar high-symmetry substrate surfaces (see, e.g., Refs. 22, 35, and 36), we are in the favorable situation that the parameter correlations were reasonably low ($|C|<0.6$), with only a few above this value, leading to rapid fit convergence and small standard deviations of the fit parameters.

Excellent fits as represented by the solid lines could be achieved in all cases. The fit quality is measured by the unweighted residuum (R_u) and the goodness of fit (GOF) parameter, the latter taking into account the difference between the number of data points and the number of parameters.[37] Excellent values for R_u in the range between 0.06 and 0.08 and for GOF between 0.8 and 1.2 were achieved, leaving only little room for further improvements.

Schematic side views of the structure models before and after annealing are shown in Fig. 4 for the TD sample and in

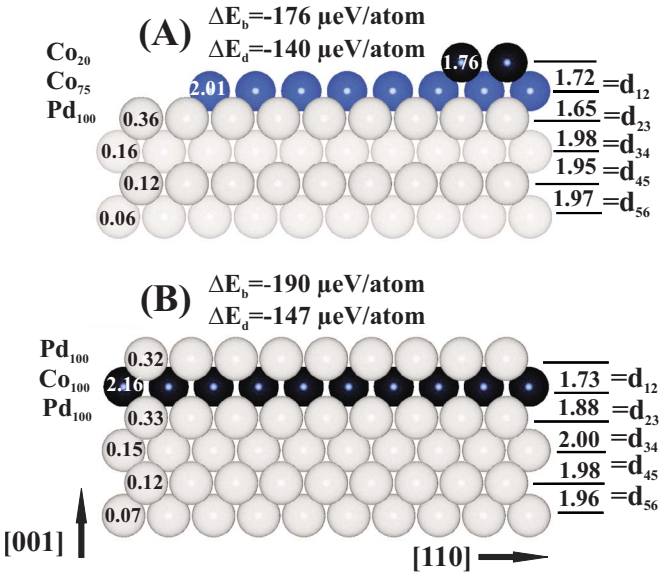

FIG. 4. (Color online) Structure model for 1 ML Co/Pd(001) using TD (A) before and (B) after annealing at 600 K for 15 min. Dark and bright balls represent Co and Pd atoms, respectively. The layer stoichiometry is given on the left; interlayer distances in Å on the right. Numbers within the spheres label the calculated local magnetic moments in Bohr magnetons. ΔE_b and ΔE_d indicate the calculated band-energy and dipole-energy contributions to the magnetic anisotropy energy, respectively.

Fig. 5 for the PLD sample. Dark and bright balls represent Co and Pd atoms, respectively. In order to properly sketch the alloy concentration within the layers, several unit cells along the [110] direction are displayed. The layer compositions are listed on the left-hand side, where the subscripts indicate the occupancy in percent of a monolayer. Since superstructure reflections were not observed, the alloy structures are disordered, preserving the overall (1×1) lattice periodicity of the Pd(001) substrate. Distances between layers i and j (d_{ij}) are given in angstrom units on the right-hand side. The numbers within the spheres represent the calculated magnetic moments in Bohr magnetons (μ_B), see below.

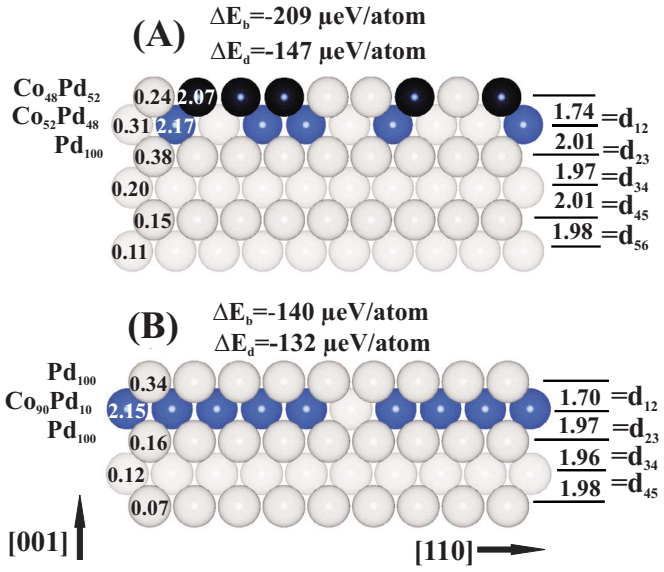

FIG. 5. (Color online) SXRD-derived structure model for 1 ML Co/Pd(001) using PLD (A) before and (B) after annealing at 600 K for 15 min. The meaning of the labels is the same as in Fig. 4.

As qualitatively discussed above, TD and PLD lead to different interface structures. In the case of TD, growth of a Co overlayer without alloying is observed. By contrast, samples prepared by PLD are characterized by substantial alloying (the error bar for the determination of the alloy concentration is about 10% per layer).

Significant relaxations are observed for those interlayer distances, where pure Co and Co-alloy layers are involved. We find values between 1.65 and 1.74 Å, corresponding to a contraction of up to 7% with respect to the bulk spacing in fcc-Co (1.77 Å) and as much as 15% relative to bulk Pd (1.95 Å).[38]

These values can be compared with predictions using elasticity theory: The fcc-Co structure with an equilibrium lattice constant of 2.50 Å laterally adapts to the Pd lattice (2.75 Å), corresponding to a 10% in-plane strain. Using Poisson's ratio for fcc-Co [$\nu=0.40$ (Ref. 39)] and the equation $\varepsilon_3/(\varepsilon_1+\varepsilon_2)=-\nu/(1-\nu)$ with $\varepsilon_1=\varepsilon_2=+0.1$, one finds $\varepsilon_3\approx-0.13$; i.e., the normal lattice spacing between the top Co layers is calculated to decrease by 13%, roughly a factor of 2 larger than experimentally derived (7%). This might be interpreted as an "unusual" interlayer expansion, but it should be kept in mind that bulk elastic data might not be appropriate for the description of thin-film elastic properties. Therefore, this approach might seem to be of limited validity, although recent work on ML strain clearly indicates that continuum elasticity may provide a meaningful estimation of lattice spacings in favorable cases, even in the ML regime.[36,40,41]

However, as far as the deeper-lying alloy layers and the pure Pd layers are concerned, there is some evidence for an unusual interlayer expansion. In this regime, an outward relaxation relative to bulk ($d_{\mathrm{Pd}}=1.945$ Å) is observed, in general. In some cases, it is quite significant and a maximum value of 2.01 Å corresponding to $\Delta d/d_{\mathrm{Pd}}=+3.3\%$ is determined (see Fig. 5).

From previous investigations, it is known that hydrogen adsorption induces an expansion of the top Pd interlayer spacings.[42–45] In the most recent quantitative LEED and SXRD study,[45] a systematic analysis of the Pd top layer expansion was carried out. For Pd(001) covered completely by hydrogen in hollow sites, an expansion of $\Delta d_{12}=4.7\pm1.0\%$ was determined. This value is somewhat larger than reported in previous LEED experiments on the "clean" Pd(001) surface [2.5% (Ref. 42), 3% (Ref. 43), and 4.6% (Ref. 44)], but smaller than the average SXRD value of 6.5%. A recent theoretical study[46] pointed out that these discrepancies can be related to different hydrogen coverages, depending on sample preparation.

In conclusion, we suggest that the observed expansion of the layer spacings could be related to dissolved hydrogen within the near-surface region. It further shows that our precise structure analysis provides evidence—albeit indirectly—for the "hydrogen problem," which is always present in common UHV studies, but hardly considered in detail, mostly because of the difficulty to detect hydrogen.

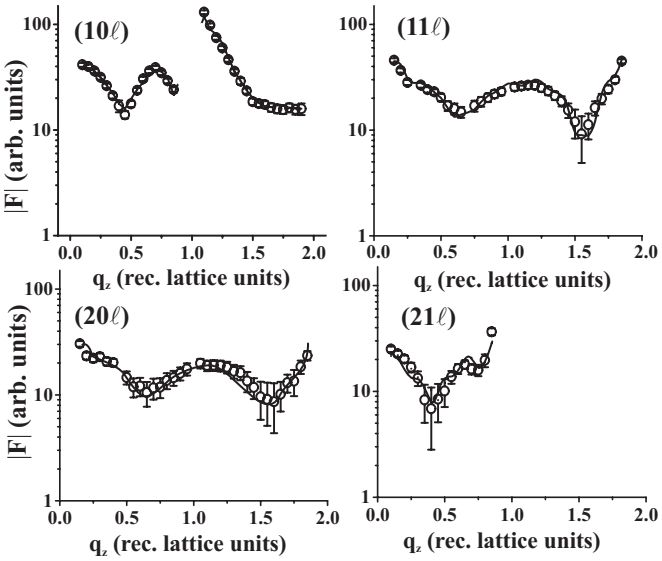

FIG. 6. Measured (symbols) and calculated (lines) structure factor amplitudes for 2 ML PLD-grown Co after annealing at 600 K for 15 min.

In the following, the SXRD analysis on the annealed samples is summarized. Annealing at 600 K induces substantial structural reorganization in both the TD and PLD samples. The corresponding structure models are shown in the lower panels (B) of Figs. 4 and 5. The Co monolayer is sandwiched between the Pd(001) substrate and the topmost Pd layer. The Pd/Co/Pd(001) layer sequence (locally) corresponds to the stacking scheme in the CuAu-($L1_0$)-type structure. Within the error bar of the composition determination, there is no difference between the annealed TD and PLD samples. The calculated structure factor amplitudes (solid lines) fit the experimental ones in all details. Unweighted residuals as low as R_u=0.06 [GOF=0.9 (Ref. 37)] are achieved.

For comparison, we have also investigated a PLD sample, where 2 ML Co were deposited followed by annealing at 600 K. Figure 6 shows the corresponding CTR's and the fits. Qualitatively, the more oscillatory distribution of the structure factor amplitude along q_z indicates a more contrasted electron density as compared to the 1 ML samples. A very good fit is also achieved ($R_u \approx 0.07$, GOF=1.2) in this case. The corresponding structure model is sketched in Fig. 7.

Although the structure bears resemblance to the annealed 1 ML samples in that it is composed of a pure Pd surface layer followed by a pure Co layer, there is no complete restructuring in the deeper-lying parts of the surface region. We find Co concentrations of 16%, 60%, and 25% within the third, fourth, and fifth layers, respectively. This suggests that the annealing temperature has not been high enough to induce a complete separation of the Co and Pd atoms to form the completely ordered Pd/Co/Pd/Co/Pd(001) multilayer structure.

C. Magneto-optic Kerr-effect measurements

Figures 8 and 9 show the magnetization curves for the TD and PLD samples before (left panels) and after annealing

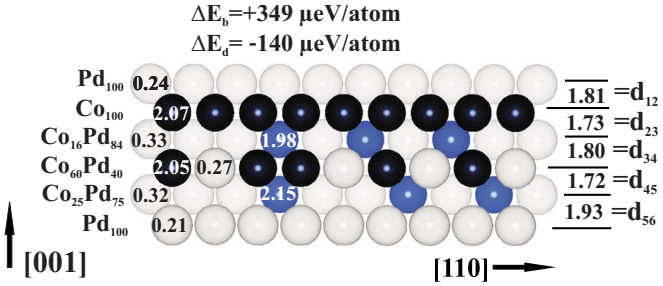

FIG. 7. (Color online) SXRD-derived structure model for 2 ML PLD-grown Co/Pd(001) after annealing at 600 K for 15 min. The meaning of the labels is the same as in Fig. 4.

(right panels). The upper curves correspond to the Kerr signals measured in the longitudinal geometry, while the lower ones show the Kerr signals observed in polar geometry. Immediately after deposition, both TD- and PLD-grown 1.1-ML-thick Co films on Pd(001) do not show perpendicular magnetization and no polar Kerr signal is detected. The larger coercivity of the TD-grown sample as compared to the PLD-grown sample is attributed to a slightly smaller thickness of the former one. In the coverage regime of around 1 ML, the coercivity sensitively depends on the Co thickness, and below about 0.7 ML, polar loops could not be measured due to the increase of coercivity above the maximum magnetic field which can be applied in the experimental setup (0.8 T).

Annealing at 600 K induces a reorientation of the easy-axis magnetization from in plane to out of plane, as evidenced by the rectangular polar loops on the lower right in Figs. 8 and 9 measured for the 1.1-ML-thick Co films on Pd(001). The perpendicular anisotropy and easy axis of magnetization pointing out of the film plane can be directly correlated with the structural reorganization leading to the for-

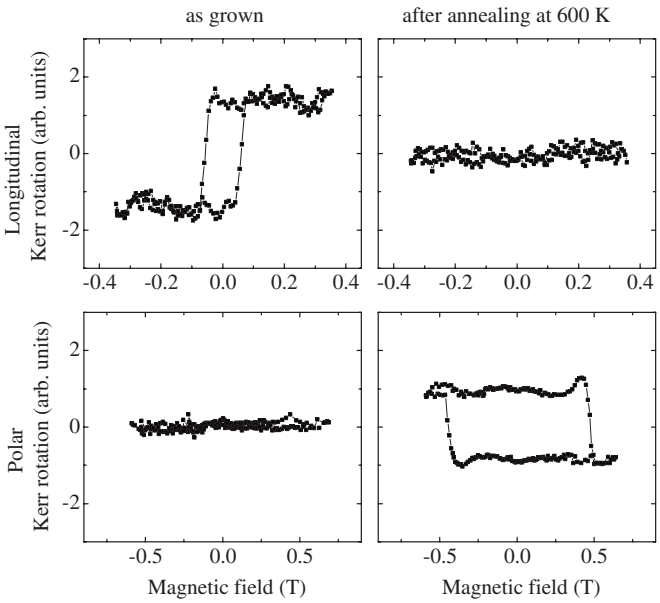

FIG. 8. Longitudinal (upper panel) and polar (lower panel) MOKE loops measured for 1.1-ML-thick Co films deposited by TD on Pd(001) before (left) and after (right) annealing at 600 K.

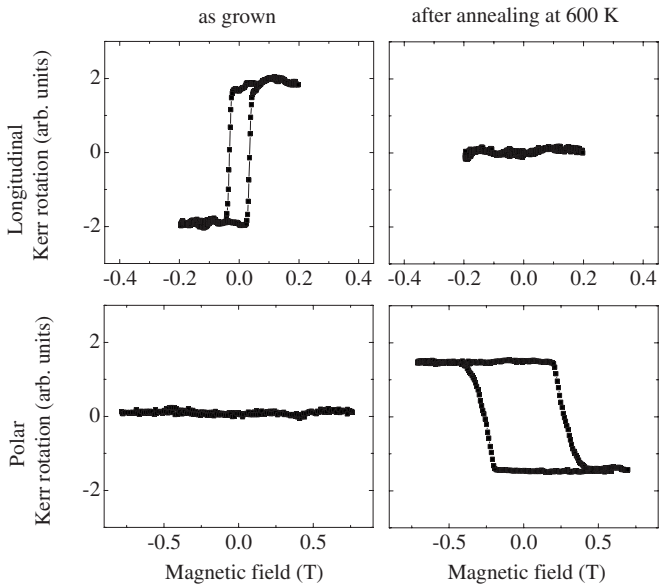

FIG. 9. Longitudinal (upper panel) and polar (lower panel) MOKE loops measured for 1-ML-thick Co films deposited by PLD on Pd(001) before (left) and after (right) annealing at 600 K.

mation of the ordered sandwich structure. By contrast, the disordered alloy found for the as-deposited PLD sample is associated with in-plane magnetization. SXRD and MOKE results nicely correlate.

In the case of the 2-ML-thick Co film (not shown), the situation is very similar: immediately after deposition only the longitudinal Kerr signal is detected, whereas the polar Kerr loop appears after annealing at 600 K. As known from the SXRD analysis, annealing the 2-ML-thick Co film leads to an ordered Pd/Co double layer above several disordered CoPd-alloy layers. The perpendicular magnetic anisotropy introduced to the system (by formation of the ordered Co-Pd alloy at the Co/Pd interface) seems to be relatively strong since 600 K annealing induces PMA up to the thickness of about 4 ML of Co.

For 600 K annealed samples, "reversed" Kerr rotation loops are observed up to 2.7 ML coverage; i.e., a negative Kerr rotation is detected in saturation in positive magnetic field.[47] The reversed polar loops can be attributed to the negative polar Kerr rotation contribution from the interface part of the Co film. The experimental evidence for a negative polar Kerr rotation detected for Co atoms in a Pd-rich environment is supported by *ab initio* band-structure calculations for the Co/Pd multilayer structure.[48] When the contribution from the noninterface part of the film dominates, the polar MOKE loops change sign and become normal [above a thickness of 2.7 ML in the case of Co grown on Pd(001)].

IV. THEORY

In order to compare the experimentally established relation between structure and magnetization with theoretical predictions, *ab initio* numerical simulations within DFT were carried out. We used the scalar-relativistic KKR method for layered systems based on the screening transformation of the structure constants which accurately describe semi-infinite systems.[49] To obtain a good convergence, we used nine Pd layers for the substrate and four empty layers for vacuum. The Madelung potential was calculated using proper boundary conditions and the estimated work function varies from 4.25 to 4.85 eV depending on the geometry and occupancy of the samples. Disorder and partial occupations within the films were treated using the single-site coherent-potential approximation (CPA). Electronic structure calculations were carried out self-consistently within the atomic sphere approximation, using the local spin-density approximation using the Perdew-Wang exchange-correlation potential.[50]

The magnetic moments in units of Bohr magnetons (μ_B) calculated for the different structures are indicated by the numbers inside the spheres of the structure models in Figs. 4, 5, and 7. Pd atoms in proximity to Co atoms acquire a finite magnetic moment in agreement with other theoretical studies.[48] Magnetic moments are at a maximum (up to $0.38\mu_B$) in Pd layers adjacent to Co layers and within the Co_xPd_{1-x} alloy layers, but rapidly decrease along the direction into the interior of the crystal.

The sixth Pd layer from the Pd/Co interface is completely nonmagnetic. The finite Pd magnetic moment is attributed to the hybridization between *d* states of Co and Pd atoms. However, the magnetic moments of Pd obtained in our study are systematically larger as reported in Ref. 48, where Co/Pd multilayers were studied using unrelaxed interlayer fcc-Pd distances (1.945 Å). In contrast to this work, our SXRD analysis shows that the distances between the Co and Pd layers are smaller by 10%–15%, leading to a stronger hybridization and to a larger polarization of the Pd atoms.

The Co $3d$–Pd $4d$ hybridization is also responsible for the enhancement of the magnetic moment of Co (maximum of $2.17\mu_B$ relative to the bulk value of $1.75\mu_B$ in fcc-Co), if it is located between Pd layers, while a slightly lower magnetic moment (1.76, 2.01, and $2.07\mu_B$, see Figs. 4 and 5) is calculated for Co surface atoms.

The self-consistent potentials were further used for the calculation of the MAE within the framework of the magnetic force theorem. For this purpose, a fully relativistic spin-polarized layer Korringa-Kohn-Rostoker method was applied, yielding the layer- and species-resolved spectral function, from which the MAE is calculated (see details, for example, in Ref. 51). The MAE calculations were carried out for two collinear magnetic configurations: $\vec{M}_{(\parallel)}$ with all local magnetic moments aligned parallel to the layers and $\vec{M}_{(\perp)}$ with all local magnetic moments aligned perpendicular to the layers. Hence, noncollinear magnetic configurations are not considered, but structural disorder is taken into account by means of the single-site CPA.

The MAE consists of two contributions. The band-energy contribution (ΔE_b) is obtained from the spectral function, summing the contributions from all layers with nonvanishing magnetic moment. The magnetic dipole-dipole anisotropy energy (ΔE_d) is computed by the Ewald summation as outlined in Ref. 52. The calculated values of ΔE_b and ΔE_d for the different structures are indicated next to the corresponding structure models in Figs. 4, 5, and 7.

At first we concentrate on the 1 ML samples. For the as-grown structures, the negative value of the band energies

($-209\ \mu$eV/atom $\leq \Delta E_b \leq -140\ \mu$eV/atom) indicates *in-plane orientation* in agreement with experiment. The differences between the ΔE_b's are due to the different geometric structures. This is most obvious for the as-grown PLD sample, characterized by a disordered 2 ML alloy related to $\Delta E_b = -209\ \mu$eV/atom corresponding to the strongest in-plane magnetization [Fig. 5(a)]. Since ΔE_d always wants to turn the magnetization in plane, the total MAE is also negative in any case. Calculated values for ΔE_d are in the $-140\ \mu$eV/atom range, as indicated in the figures. The small variation of ΔE_d is due to slightly different Co concentrations taken from the SXRD analysis. For the annealed 1 ML samples, negative values for ΔE_b are found as well (-190 and $-140\ \mu$eV/atom); i.e., an in-plane orientation is also predicted for the Pd/Co/Pd(001) sandwich structure, which is at variance with experiment.

The annealed 2 ML structure is the only one where a positive band energy is calculated [see Fig. 7(b)]. It is equal to $+349\ \mu$eV/atom and, since the dipole contribution ΔE_d is equal to $-140\ \mu$eV/atom, the total MAE is positive ($+209\ \mu$eV/atom) indicating out-of-plane PMA, in agreement with experiment.

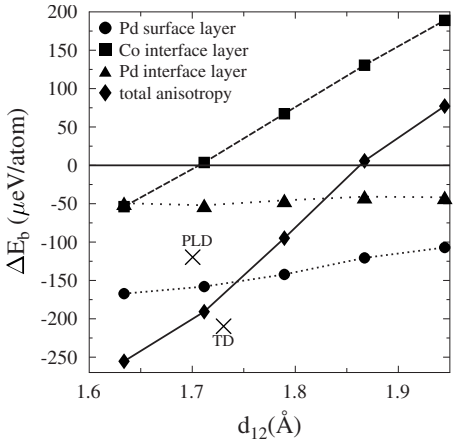

FIG. 10. Layer-resolved band-energy contributions to the MAE in Pd/Co/Pd(001) versus Pd/Co interlayer distance (d_{12}). Contributions of the Pd top layer, the Co layer, and the Pd interface layer are represented by circles, squares, and triangles, respectively. Diamonds represent the total band energy. Crosses labeled by TD and PLD indicate the calculated ΔE_b's for the annealed samples on the basis of the SXRD structure parameters. Lines are guides for the eyes.

V. DISCUSSION

The SXRD analysis of 1 ML Co deposited on Pd(001) by TD and PLD has revealed distinct differences between the structures (fct Co overlayer versus formation of a CoPd alloy). Annealing at 600 K for 15 min induces a restructuring, leading to the formation of a Pd/Co/Pd(001) sandwich structure independent of the deposition method. Simultaneously, MOKE experiments indicate a spin-reorientation transition from in-plane to out-of-plane magnetization.

Although the calculations derive negative values of ΔE_b for the as-deposited 1 ML samples in agreement with experimental observation, they do not predict the experimentally observed perpendicular magnetization after formation of the Pd/Co/Pd(001) sandwich. The discrepancy between theory and experiment with regard to the annealed 1 ML samples might be attributed to details of the experiments. A possible scenario is the influence of hydrogen adsorbed at the surface and/or dissolved in the near-surface region. In typical UHV experiments, hydrogen "contamination" is a notorious problem, hardly controllable and difficult to detect. Moreover, especially Pd is known to efficiently dissolve hydrogen, and recent investigations have clarified in detail the relation between hydrogen adsorption and top-layer spacings.[45,46]

As outlined in Sec. III, the SXRD analysis provides some evidence for hydrogen contamination, albeit indirectly, by expanded lattice spacings. Numerous examples are known, where adsorption of a foreign species including metals and hydrogen is related to a change of the easy-axis magnetization (see, e.g., Refs. 40 and 53–57). In general, the spin reorientation is attributed to the change of the surface anisotropy, which in the case of hydrogen adsorbed on Ni/Cu(001) could be correlated with a relaxation of the Ni top-layer spacing.[40,56]

Nevertheless, the relation of the band energies with the structure models reveals some trends. While in the case of the TD sample there is only a small difference between the ΔE_b's before and after annealing (-176 versus $-190\ \mu$eV/atom, respectively), a much larger difference exists for the PLD sample. We find $\Delta E_b = -209\ \mu$eV/atom for the as-deposited disordered alloy structure [Fig. 5(a)] corresponding to the strongest tendency for in-plane magnetization of all samples. After annealing which leads to the formation of the ordered sandwich structure, ΔE_b is equal to $-140\ \mu$eV/atom [Fig. 5(b)]. Although ΔE_b is still negative, the change from -209 to $-140\ \mu$eV/atom indicates that there is some trend for out-of-plane magnetization upon formation of the Pd/Co/Pd(001) sandwich structure. This conclusion is supported by the strongly positive band energy of $+349\ \mu$eV/atom for the (still slightly disordered) Pd/Co/Pd/Co/Pd(001) multilayer structure prepared by annealing 2 ML PLD-grown Co/Pd(001). This indicates that the contribution of the Co-Pd interface to the MAE is decisive for the PMA.[6]

In order to elucidate the contribution of relaxations to ΔE_b, we have carried out calculations for the Pd/Co/Pd(001) system: the interlayer distances within the Pd substrate and the distance from the substrate to the Co layer (the latter labeled by d_{23} in Figs. 4 and 5) were assumed to be unrelaxed, i.e., fcc-like corresponding to $d = 1.945$ Å. Only the distance between the top Pd layer and the Co layer (d_{12}) was varied between 1.630 Å and $d_{\mathrm{Pd}} = 1.945$ Å. In Fig. 10, the diamonds represent the calculated total band energy ΔE_b. From the slope of the curve, it is evident that a contraction of the top interlayer distance leads to a negative total band-energy contribution, i.e., an increased Co-Pd hybridization favors in-plane magnetization.

Within the Bruno model, the magnetocrystalline anisotropy is determined by the orbital moment and, consequently, influenced by hybridization of electronic states.[58] For a small Co-Pd interlayer distance, the orbital moment is quenched

(no PMA), whereas for a large interlayer distance, it is sizable (PMA), in agreement with our theoretical findings.

In Fig. 10, squares, triangles, and circles represent the layer-resolved contributions to ΔE_b from the Co and adjacent Pd layers, respectively. The strongest contribution to ΔE_b comes from the Co layer. For d_{12} larger than about 1.70 Å, a positive contribution from the Co layer is derived [note that for the experimentally derived value of d_{12} (1.73 and 1.70 Å) the Co band-energy contribution is almost zero]. By contrast, the ΔE_b's of the Pd layers adjacent to the Co layer are always negative and their dependence on d_{12} is considerably smaller.

Taking into account the SXRD-derived structures of the annealed TD and PLD samples in all details does not lead to significantly changed ΔE_b's as compared to the model calculations. In Fig. 10, the corresponding values are indicated by crosses and are labeled by "TD" and "PLD," respectively.

An increased tendency for in-plane magnetization with decreasing layer distance is in agreement with considerations based on magnetoelasticity: CoPd alloys with intermediate Co concentration are characterized by a strongly positive magnetostriction coefficient (e.g., $\frac{3}{2}\lambda_{100}=1.25\times10^{-4}$ for a Co concentration of 50%).[59] Assuming that bulk values can be applied to the thin-film structure—at least as far as the sign is concerned—a positive magnetostriction coefficient favors in-plane magnetization when the film is laterally expanded and vertically contracted (for details, see Ref. 60).

We can compare the result for ΔE_b at $d_{12}=d_{\mathrm{Pd}}$ to the study of Pustogowa *et al.*[11] In Ref. 11 an (unrelaxed) fcc-Pd/Co/Pd(001) sandwich structure was assumed and a (negative) band-energy contribution of only $\Delta E_b=-25$ μeV was calculated. For the same geometry, we obtained a positive band energy $\Delta E_b=75$ μeV. The discrepancy with the work of Pustogowa *et al.*[11] can be explained by the high sensitivity of ΔE_b of ultrathin films to the integration over the Brillouin zone. In our calculations we used a very accurate adaptive mesh refinement method,[61] which can provide accuracy up to 1 μeV for MAE calculations.[62]

VI. SUMMARY

We have presented a combined experimental and theoretical study of the correlation between geometric structure and magnetic properties of 1- and 2-ML-thick Co films grown on Pd(001) by TD and PLD. While for the as-deposited samples substantial differences between the interface structures depending on the preparation method are determined (epitaxial growth of fct-Co for TD versus formation of a disordered $\mathrm{Co}_x\mathrm{Pd}_{1-x}$ alloy in the case of PLD), annealing induces a structural reorganization to a Pd/Co/Pd sandwich structure with Pd floating on top. This goes in parallel with a reorientation of the easy magnetization axis from in plane to out of plane. While calculations predict an in-plane easy axis for the as-deposited samples in agreement with experiment, the PMA observed for the lattice relaxed Pd/Co/Pd(001) sandwich is not confirmed. Calculations indicate that the reduction of the Pd/Co interlayer spacing increases the tendency for in-plane magnetization due to the stonger Co $3d$–Pd $4d$ hybridization.

A strong tendency for PMA in the case of the (not completely ordered) double sandwich structure [Pd/Co/Pd/Co/Pd(001)] is determined, emphasizing the decisive importance of structural order and the interface contribution to the magnetic anisotropy energy.

ACKNOWLEDGMENTS

The authors acknowledge helpful discussions with J. Barthel and X. F. Jin. Technical support by W. Greie is also acknowledged. Calculations were carried out at the Rechenzentrum Garching.

*Electronic address: hmeyerhm@mpi-halle.mpg.de

[1] L. M. Falicov, D. T. Pierce, S. D. Bader, R. Gronski, K. B. Hathaway, H. J. Hopster, D. N. Lambeth, S. S. P. Parkin, G. Prinz, M. Salamon, I. K. Schuller, and R. H. Victora, J. Mater. Res. **5**, 1299 (1990).

[2] T. Wakiyama, in *Physics and Engeneering Applications of Magnetism*, edited by Y. Ishikawa and N. Miura (Springer Verlag, Berlin, 1991), p. 133.

[3] D. Weller, H. Brändle, G. Gorman, C.-J. Lin, and H. Notarys, Appl. Phys. Lett. **61**, 2726 (1992). D. Weller, H. Brändle, and C. Chappert, J. Magn. Magn. Mater. **121**, 461 (1993).

[4] M. Maret, M. C. Cadeville, R. Poinsot, A. Herr, E. Beaurepaire, and C. Monier, J. Magn. Magn. Mater. **166**, 45 (1997).

[5] W. Grange, M. Maret, J.-P. Kappler, J. Vogel, A. Fontaine, F. Petroff, G. Krill, A. Rogalev, J. Goulon, M. Finazzi, and N. B. Brookes, Phys. Rev. B **58**, 6298 (1998).

[6] B. N. Engel, C. D. England, R. A. Van Leeuwen, M. H. Wiedmann, and C. M. Falco, Phys. Rev. Lett. **67**, 1910 (1991).

[7] S. T. Purcell, M. T. Johnson, N. W. E. McGee, J. J. de Fries, W. B. Zeper, and W. Hoving, J. Appl. Phys. **73**, 1360 (1993).

[8] J. Dorantes-Davila, H. Dreysse, and G. M. Pastor, Phys. Rev. Lett. **91**, 197206 (2003).

[9] S. S. A. Razee, J. B. Staunton, B. Ginatempo, F. J. Pinski, and E. Bruno, Phys. Rev. Lett. **82**, 5369 (1999).

[10] G. Hadjipanayis and P. Gaunt, J. Appl. Phys. **50**, 2358 (1979).

[11] U. Pustogowa, C. Blaas, C. Uiberacker, J. P. Weinberger, L. Szunyogh, and C. Sommers, Eur. Phys. J. B **16**, 653 (2000).

[12] D.-S. Wang, R. Wu, and A. J. Freeman, Phys. Rev. B **48**, 15886 (1993).

[13] D.-S. Wang, R. Wu, and A. J. Freeman, J. Appl. Phys. **75**, 6409 (1994).

[14] We use the primitive surface (s) setting of the unit cell, which is related to the face-centered setting of the bulk (b) by the following relations: $[100]_s=(1/2)([100]_b-[010]_b)$, $[010]_s=(1/2)\times([100]_b+[010]_b)$, *and* $[001]_s=[001]_b$.

[15] J. M. MacLaren and R. H. Victora, J. Appl. Phys. **76**, 6069 (1994).

[16] R. H. Victora and J. M. MacLaren, Phys. Rev. B **47**, 11583 (1993).

[17] S.-K. Kim, V. A. Chernov, J. B. Kortright, and Y. M. Koo, Appl.

Phys. Lett. **71**, 66 (1997).
[18] S.-K. Kim and S.-C. Shin, J. Appl. Phys. **89**, 3055 (2001).
[19] S.-K. Kim, Y. M. Koo, V. A. Chernov, J. B. Kortright, and S.-C. Shin, Phys. Rev. B **62**, 3025 (2000).
[20] H. Giordano, A. Atrei, M. Torrini, U. Bardi, M. Gleeson, and C. Barnes, Phys. Rev. B **54**, 11762 (1996).
[21] A. Atrei, H. Giordano, M. Torrini, U. Bardi, M. Glesson, and C. Barnes, Surf. Rev. Lett. **4**, 1123 (1997).
[22] H. L. Meyerheim, V. Stepanyuk, A. L. Klavsyuk, E. Soyka, and J. Kirschner, Phys. Rev. B **72**, 113403 (2005).
[23] J. T. Kohlhepp, G. J. Strijkers, H. Wieldraaijer, and W. J. M. de Jonge, Phys. Status Solidi A **189**, 701 (2002).
[24] Y. Fujii, T. Komine, T. Kai, and K. Shiiki, J. Phys.: Condens. Matter **11**, 9601 (1999).
[25] H.-U. Krebs, Int. J. Non-Equilib. Process. **10**, 3 (1997).
[26] J. Shen, Z. Gai, and J. Kirschner, Surf. Sci. Rep. **52**, 163 (2004).
[27] K. Sato, Jpn. J. Appl. Phys. **20**, 2403 (1981).
[28] M. Bloch, J. Appl. Crystallogr. **18**, 33 (1985).
[29] F. Kretschmar, D. Wolf, H. Schulz, H. Huber, and H. Plockl, Z. Kristallogr. **178**, 130 (1987).
[30] R. Feidenhans'l, Surf. Sci. Rep. **10**, 105 (1989).
[31] I. K. Robinson and D. J. Tweet, Rep. Prog. Phys. **55**, 599 (1992).
[32] I. K. Robinson, Phys. Rev. B **33**, 3830 (1986).
[33] E. Vlieg, J. Appl. Crystallogr. **30**, 532 (1997).
[34] Edward Prince, *Mathematical Techniques in Crystallographic Computing* (Springer, Berlin, 1994).
[35] H. L. Meyerheim, R. Popescu, D. Sander, J. Kirschner, O. Robach, and S. Ferrer, Phys. Rev. B **71**, 035409 (2005).
[36] H. L. Meyerheim, E. Soyka, and J. Kirschner, Phys. Rev. B **74**, 085405 (2006).
[37] R_u is defined as $R_u=\Sigma||F_{obs}|-|F_{calc}||/\Sigma|F_{obs}|$, where F_{obs} and F_{calc} are the observed and calculated structure factors, respectively, and the summation runs over all data points; for the definition of the GOF, see Refs. 30 and 31
[38] The error bar for the distance determination is in the range between 0.05 and 0.10 Å.
[39] R. F. S. Hearmon, *The Elastic Constants of Crystals and Other Anisotropic Materials*, Landolt-Börnstein, New Series, Group III, Vol. 18, supplement to III/11 (Springer, Berlin, 1984).
[40] D. Sander, W. Pan, S. Ouazi, J. Kirschner, W. Meyer, M. Krause, S. Müller, L. Hammer, and K. Heinz, Phys. Rev. Lett. **93**, 247203 (2004).
[41] E. Groppo, C. Prestipino, C. Lamberti, P. Luches, C. Giovanardi, and F. Boscherini, J. Phys. Chem. B **107**, 4597 (2003).
[42] R. J. Behm, K. Christman, G. Ertl, M. A. Van Hove, P. A. Thiel, and W. H. Weinberg, Surf. Sci. **88**, L59 (1979).
[43] J. Quinn, Y. S. Li, D. Tian, H. Li, F. Jona, and P. M. Marcus, Phys. Rev. B **42**, 11348 (1990).
[44] J. Burchhardt, E. Lundgren, M. M. Nielsen, J. N. Andersen, and D. L. Adams, Surf. Rev. Lett. **3**, 1339 (1996).
[45] S. H. Kim, H. L. Meyerheim, J. Barthel, J. Kirschner, J. Seo, and J. S. Kim, Phys. Rev. B **71**, 205418 (2005).
[46] S. C. Jung and M. H. Kang, Phys. Rev. B **72**, 205419 (2005).
[47] M. Przybylski, L. Yan, J. Zukrowski, M. Nyvlt, Y. Shi, A. Winkelmann, J. Barthel, M. Wasniowska, and J. Kirschner, Phys. Rev. B **73**, 085413 (2006).
[48] S. Uba, L. Uba, A. N. Yaresko, A. Ya. Perlov, V. N. Antonov, and R. Gontarz, J. Phys.: Condens. Matter **10**, 3769 (1998).
[49] K. Wildberger, R. Zeller, and P. H. Dederichs, Phys. Rev. B **55**, 10074 (1997).
[50] J. P. Perdew and Y. Wang, Phys. Rev. B **45**, 13244 (1992).
[51] J. Henk, A. M. N. Niklasson, and B. Johansson, Phys. Rev. B **59**, 9332 (1999).
[52] L. Szunyogh, B. Ujfalussy, and P. Weinberger, Phys. Rev. B **51**, 9552 (1995).
[53] R. Vollmer, Th. Gutjahr-Löser, J. Kirschner, S. van Dijken, and B. Poelsema, Phys. Rev. B **60**, 6277 (1999).
[54] S. D. Bader and J. L. Erskine, in *Ultrathin Magnetic Structures II*, edited by J. A. C. Bland and B. Heinrich (Springer, Berlin, 1994), Chap. 4
[55] H. J. Elmers and U. Gradmann, Appl. Phys. A: Solids Surf. **51**, 255 (1990).
[56] F. Máca, A. B. Schick, G. Schneider, and J. Redinger, J. Magn. Magn. Mater. **272**, 1194 (2004).
[57] H. L. Meyerheim, D. Sander, R. Popescu, J. Kirschner, O. Robach, and S. Ferrer, Phys. Rev. Lett. **93**, 156105 (2004).
[58] P. Bruno and J.-P. Renard, Appl. Phys. A: Solids Surf. **49**, 499 (1989).
[59] H. Fujiwara, H. Kadomatsu, and T. Tokunaga, J. Magn. Magn. Mater. **31-34**, 809 (1983).
[60] D. Sander, Rep. Prog. Phys. **62**, 809 (1999).
[61] J. Henk, Phys. Rev. B **64**, 035412 (2001).
[62] S. Ostanin, J. B. Staunton, S. S. A. Razee, C. Demangeat, B. Ginatempo, and E. Bruno, Phys. Rev. B **69**, 064425 (2004).